1-2001

White Dwarfs in Common Proper Motion Binary Systems: Mass Distribution and Kinematics

Nicole M. Silvestri
Florida Institute of Technology

Terry D. Oswalt
Florida Institute of Technology, oswaltt1@erau.edu

Matt A. Wood
Florida Institute of Technology

J. Allyn Smith
University of Michigan

I. Neill Reid
University of Pennsylvania

See next page for additional authors

THE ASTRONOMICAL JOURNAL, 121:503–516, 2001 January

WHITE DWARFS IN COMMON PROPER MOTION BINARY SYSTEMS: MASS DISTRIBUTION AND KINEMATICS

NICOLE M. SILVESTRI, TERRY D. OSWALT,[1,2,3,4] AND MATT A. WOOD
Department of Physics and Space Sciences and the SARA Observatory, Florida Institute of Technology, Melbourne, FL 32901-6975; nicole@luyten.astro.fit.edu, oswalt@luyten.astro.fit.edu, wood@astro.fit.edu

J. ALLYN SMITH[1,2,5,6]
Department of Physics, 2477 Randall Laboratory, University of Michigan, 500 East University, Ann Arbor, MI 48109-1120; jasmith@sdss3.physics.lsa.umich.edu

I. NEILL REID[3]
Department of Physics and Astronomy, University of Pennsylvania, 209 South 33d Street, Philadelphia, PA 19104-6396; inr@hep.upenn.edu

AND

EDWARD M. SION
Department of Astronomy and Astrophysics, Villanova University, 800 Lancaster Avenue, Villanova, PA 19085; emsion@ast.vill.edu
Received 2000 March 2; accepted 2000 September 20

ABSTRACT

We present the mass distribution, gravitational redshifts, radial velocities, and space motions of white dwarf stars in common proper motion binary systems. The mass distribution we derive for the 41 DA white dwarfs in this study has a mean of $0.68 \pm 0.04\ M_{\odot}$. This distribution has a slightly higher mean and larger dispersion than most previous white dwarf studies. We hypothesize that this is due to a higher fraction of cool (average $T_{\rm eff} \sim 10{,}000$ K), hence old, white dwarfs in our sample. Our results indicate that samples made up of predominantly cool, old white dwarf stars tend to have a bimodal distribution with a second mass peak at $\sim 1.0\ M_{\odot}$, which skews the mean toward a higher mass. Both the mean and individual white dwarf masses we report here are in better agreement with those determined from model atmosphere spectroscopic fits to line profiles than with most previous gravitational redshift studies of cool white dwarfs. Our results indicate that measurement biases and weak geocoronal emission lines in the observed spectra may have affected previous gravitational redshift measurements. These have been minimized in our study. We present measurements for some previously unobserved white dwarfs, as well as independent new measurements for some that have been reported in the literature. A list of complete space motions for 50 wide binary white dwarfs is presented, derived from radial velocity measurements of their nondegenerate companions. We find that the UVW space motions and dispersions of the common proper motion binaries that contain white dwarf components are consistent with those of old, metal-poor disk stars.

Key words: stars: fundamental parameters — stars: kinematics — techniques: spectroscopic — white dwarfs

1. INTRODUCTION

White dwarf (WD) stars are the final evolutionary stage for the vast majority of all stars. They preserve clues to the evolution of the Galaxy and its star formation history. They are a fairly homogeneous class of stars, with average radii of ~ 8500 km, mean densities on the order of 10^6 g cm^{-3}, and typical surface temperatures ranging from the hottest at $\sim 100{,}000$ K to the coolest at ~ 3000 K.

The shape of the WD mass distribution yields important information about Galactic evolution and the late stages of stellar evolution (Wegner & Reid 1987). As products of post–asymptotic giant branch evolution, the mass distribution for WDs with companions also provides useful constraints on wide binary orbital evolution and post–main-sequence mass loss as a function of spectral type (Oswalt et al. 1990).

The white dwarf luminosity function provides a firm lower limit to the age of the local Galactic disk and constrains its star formation history (see Winget et al. 1987; Liebert, Dahn, & Monet 1988; Iben & Laughlin 1989; Yuan 1989; Wood 1992, 1995; Oswalt et al. 1996; Smith 1997; Leggett, Ruiz, & Bergeron 1998). Despite the discovery of thousands of WDs since the first, Sirius B, was observed in 1860 and later explained in the 1920s (Adams 1925), fundamental WD parameters, such as individual masses, radial velocities, and complete space motions are still available for only a few objects. Since the original Hamada & Salpeter (1961) zero-temperature mass-radius configurations were developed, new static models for WD mass-radius relations (e.g., Vennes, Fontaine, & Brassard 1995), as well as improved evolutionary models for WDs (Wood 1992, 1995; Benvenuto & Althaus 1999; Hansen

[1] Visiting Astronomer, Kitt Peak National Observatory and Cerro Tololo Inter-American Observatory, National Optical Astronomy Observatories, operated by the Association of Universities for Research in Astronomy, Inc., under cooperative agreement with the National Science Foundation.

[2] Visiting Astronomer, Lowell Observatory.

[3] Visiting Astronomer, W.M. Keck Observatory, is operated as a scientific partnership among the California Institute of Technology, the University of California, and the National Aeronautics and Space Administration. The Observatory was made possible by the generous financial support of the W.M. Keck Foundation.

[4] National Science Foundation.

[5] Visiting Astronomer, McDonald Observatory, which is owned and operated by the University of Texas.

[6] Current address: Department of Physics and Astronomy, University of Wyoming, P.O. Box 3905, Laramie, WY 82071; josmith@uwlp.edu.

1999; Saumon & Jacobson 1999), have significantly improved the interpretation of observational properties of these stars. At the present time, the accuracy of individual WD mass measurements is the limiting factor in testing these models.

Gravitational redshifts offer the most direct way of testing the theoretical mass-radius relation. The first measured WD redshift was for Sirius B (Adams 1925), one of the few nearby binaries where the orbital and systemic radial velocity of the star can be dissociated from the gravitational redshift. To date, several dozen gravitational redshifts have been measured for the brighter WDs in Galactic clusters and wide binaries, most notably by Greenstein et al. (1977), Schulz (1977), Koester (1987), Wegner (1989), Wegner, Reid, & McMahan (1989), Wegner & Reid (1991), Bergeron, Liebert, & Fulbright (1995), and Reid (1996).

In this paper, we examine two pieces of the puzzle: the mass distribution and kinematics of cool WDs as determined from gravitational redshifts, and the radial velocity measurements of the WD and main-sequence (MS) components of common proper motion binaries (CPMBs), respectively. In § 2, we present the observational circumstances and reduction techniques used for the stars in this study. In § 3, we analyze the radial velocity measurements of 50 binaries containing WDs. We examine the gravitational redshifts of 41 WDs in § 4, which lead to the individual mass determinations and final mass distribution in § 5. We discuss the implications of the kinematics and space motions of the sample of 50 WDs in the solar neighborhood in § 6 and summarize our results in § 7.

2. OBSERVATIONS AND DATA REDUCTION

Our program stars were drawn primarily from the "Proper Motion Survey with the 48-Inch Schmidt Telescope" (Luyten 1963, 1969, 1974, 1979) as described by Oswalt, Hintzen, & Luyten (1988). They are CPMBs with at least one probable WD component, based on color and reduced proper motion criteria. A subset of this sample was chosen for radial velocity determinations based on prior *BVRI* photometry, spectroscopic identification of a WD component with probable Hα absorption, and effective temperature determinations (see Oswalt et al. 1988; Smith 1997). Our sample is relatively faint for high-resolution studies, with an average $V = 15.3$. For this study, each of the binary system components was observed on the same night, with the exception of LP 516-12/13 (WD 2051+095), whose components were observed approximately 24 hr apart because of the onset of twilight (if observing the same binary on two different nights we must correct for solar and Earth motion over the course of the 24 hr period).

The majority of the observations were obtained using echelle spectrographs on the 4 m telescopes at KPNO and CTIO. Additional measurements were made with the High-Resolution Echelle Spectrometer (HIRES) on the 10 m Keck I Telescope (discussed by Vogt et al. 1994; Reid 1996). Observations were made on a total of 17 nights between 1991 and 1996 (see Table 1). The grating tilt and cross-disperser for all echelle spectrographs were set to include Hα and Hβ (~3500–7200 Å). Only during the 1995 May CTIO run was a conventional non–cross-dispersed spectrograph used. In this case, both stars of each pair were placed on the slit, and the grating tilt was set to cover the full wavelength range from 3500 to 7200 Å.

The data were reduced using standard IRAF[7] reduction procedures. First, they were bias-corrected, dark-subtracted, and flat-field–normalized. Then, the orders containing Hα and Hβ were extracted and wavelength calibrated using ThAr and HeNeAr arc lamp spectra. Flux calibrations were not performed, since they are not necessary for radial velocity measurements and most nights were not photometric. Gaussian fitting routines were used to determine the centroid position of the Hα line profile for each star. A few measurements were made of each star's Hα feature (for stars where more than one image was obtained) to provide an indication of measurement precision, as the low signal-to-noise ratio (S/N) of the WD spectra made the fit highly dependent on the choice of the initial and final points. In some cases, inclusion of part of the line wings was unavoidable. The standard deviations of the multiple measurements (fully one-half of the binaries in this study were observed two to three times; these were typically the faintest of the binaries) were propagated into the error estimates for the gravitational redshifts, radial velocities, and masses.

The spectra obtained in 1991 October–November and 1992 June were plagued by strong geocoronal Hα emission due to high geomagnetic substorm activity. An attempt was made to measure the stellar Hα line cores without sky subtraction. However, the geocoronal lines imposed too much asymmetry in the stellar line profiles to allow accurate measures. The normal sky subtraction routines in IRAF proved insufficient to remove the geocoronal Hα emission. Therefore, we adopted a procedure in which a separate narrow sky spectrum was extracted within each order from above and below the "combined" (star plus sky) spectrum (Silvestri 1997). This was achieved by defining a suitable extraction aperture for the combined spectrum, then using it as a template aperture for the sky spectrum, which was offset in the cross-dispersion direction above and below the combined spectrum. Once oriented properly, the sky aperture was made as wide as possible for maximum S/N. Great care was taken to ensure that the sky spectrum did not overlap the combined spectrum, as this subtracts valuable

[7] IRAF is written and supported by the IRAF programming group at the National Optical Astronomy Observatories.

TABLE 1

JOURNAL OF OBSERVATIONS

Date	Nights	Location	Aperture	Spectrograph	CCD	Camera
1991 Oct 9–11	3	KPNO	4 m	Echelle	TI	UV
1991 Nov 15–17.....	3	CTIO	4 m	Echelle	Tek	Red
1992 Jun 29–Jul 1.....	3	CTIO	4 m	Echelle	Tek	Red
1993 Apr 28–30	3	CTIO	4 m	Echelle	Tek	Red
1995 May 5–7	3	CTIO	4 m	2D-FRUTTI	Loral	...
1996 Jun 5–6	2	Keck	10 m	Echelle	HIRES	Red

TABLE 2

MEASURED WAVELENGTHS OF Hα BEFORE AND AFTER SKY SUBTRACTION

WD Number	λ Before (Å)	λ After (Å)	Δλ (Å)	Shift (km s^{-1})
0027−545.....	6564.04	6563.57	−0.46	−21.26
0120−024.....	6562.99	6563.79	0.80	36.48
0148+641.....	6562.23	6563.42	1.19	54.26
0150−164.....	6562.36	6561.86	−0.50	−22.86
0200−170.....	...	6560.09	...	...
0204−306.....	6564.27	6564.80	0.53	24.27
0251−008.....	6563.71	6563.88	0.17	7.63
0315−011.....	6564.44	6563.92	−0.52	−23.68
0433+270.....	6564.95	6564.11	−0.84	−38.40
0443−275.....	6563.32	6563.55	0.23	10.47
0628−020.....	6562.74	6564.76	2.02	92.34
0642−285.....	6563.65	6563.66	0.01	0.37
0726+39	6560.39	6562.12	1.73	79.22
0738−172.....	6563.57	6564.12	0.55	25.23
0820−583.....	...	6563.61	...	...
0926−039.....	6562.69	6562.30	−0.386	−17.64
0935−371A.....	6561.90	6562.91	1.012	46.26
0935−371B.....	6559.96	6564.25	4.288	196.01
1043−034.....	6562.40	6562.00	−0.398	−18.19
1105−048.....	6564.61	6564.89	0.277	12.66
1148+544.....	...	6562.58	...	...
1211+392.....	...	6564.76	...	...
1214+032.....	6563.63	...	...	...
1304+227.....	6561.12	6562.61	1.49	68.29
1317−021.....	6561.04	6562.25	1.21	55.49
1327−083.....	6563.53	6563.97	0.44	20.02
1334−160.....	6565.92	6564.94	−0.98	−44.93
1337−023.....	6561.42	6566.28	4.86	222.07
1348−271.....	6565.41	6562.76	−2.65	−121.14
1354+340.....	6566.08	6563.21	−2.87	−131.19
1541−381.....	6563.06	6564.33	1.27	58.24
1544+005.....	6561.86	6561.75	−0.11	−4.89
1544−377.....	6562.98	6563.63	0.65	29.71
1550+716.....	6562.77	6563.43	0.66	30.08
1555−089.....	6563.87	6563.74	−0.13	−6.03
1618−505.....	6561.23	6561.16	−0.07	−3.15
1620−391.....	6563.33	6564.16	0.83	37.94
1623−540.....	6565.58	6565.25	−0.33	−14.95
1659−531.....	6564.16	6564.67	0.51	23.40
1716+020.....	6561.76	6561.65	−0.11	−5.12
1743−132.....	6561.76	6561.66	−0.10	−4.66
1750+098.....	6565.18	6562.02	−3.16	−144.50
1911+135.....	6562.40	6562.13	−0.27	−12.34
1917−077.....	6566.36	6564.88	−1.48	−67.79
1923+715.....	6563.76	6562.06	−1.70	−77.71
2044−043.....	6561.74	6562.78	1.04	47.54
2047+809.....	6562.42	6562.99	0.57	26.19
2051+095.....	6564.32	6563.13	−1.19	−54.53
2153−512.....	6562.34	...	...	...
2154−437.....	6562.72	6563.19	0.47	21.35
2249−105.....	...	6562.47	...	...
2253−081.....	6561.63	6562.85	1.22	55.86
2256+311.....	6562.80	...	...	...
2318+126.....	6563.97	6561.94	−2.03	−92.80
2323−241.....	6565.14	6565.24	0.10	4.66
2341+321.....	6563.13	6563.02	−0.11	−5.17
2351−333.....	6563.24	6563.24	0.00	0.05
2358+270.....	...	6563.22	...	...

counts from the faint WD spectrum and overcorrects for sky contamination.

After the combined spectrum apertures and the sky spectrum apertures were defined and extracted, the same wavelength scale was applied to both. First, the sky apertures were multiplied by a constant to account for the difference in width and effective exposure of the sky apertures (generally larger for best possible S/N) compared with the combined aperture, which was generally matched to the stellar seeing disk of ∼1″–2″. Then, the weighted sky apertures were subtracted from the summed combined spectrum to yield sky-subtracted line profiles. In most cases, this made a tremendous difference in the measured wavelength of the Hα feature, as shown in Table 2. This technique allowed us to determine the velocities for several WDs for which the line core could not previously be measured. Despite this new reduction method, there were still three WDs that could not be measured even after the sky corrections were applied (WD 1214+032, WD 2153−512, and WD 2256+311). For these WDs, the geocoronal line had made it appear that there was a measurable core. However, after elimination of the geocoronal lines the S/N of the remaining spectrum was too low to make an accurate measurement.

Table 2 demonstrates the effect of geocoronal emission on the observed location of the Hα core. Hα lines in which the red wing was "filled in" or corrupted to some extent by the geocoronal emission yielded wavelength measurements that were skewed toward bluer wavelengths and vice versa. During most of the nights of observation, the geocoronal emission fell predominantly in the red wing of the Hα absorption core, resulting in a measured wavelength that was skewed toward bluer (shorter) wavelengths (this effect depends on the component of Earth's velocity along the line of sight to the WD). The degree to which the geocoronal emission corrupts the measurement also depends on other factors, such as the intrinsic radial velocity and gravitational redshift of the Hα feature and the S/N of the spectrum. The data in Table 2 demonstrate that, on average, the removal of the geocoronal feature resulted in a larger redshift; i.e., more measurements were shifted toward higher wavelengths (red). This implies that without these corrections our individual masses would have been systematically lower than the reported values.

3. RADIAL VELOCITIES

It is difficult to separate the effect of line-of-sight velocity relative to Earth and the gravitational redshift (∼30 km s^{-1}), which are comparable in magnitude. In general, only average radial velocities are determinable for groups of individual WDs. However, many WDs are members of CPMBs. Most of these systems have such large semimajor axes ($\langle a \rangle \sim 10^3$ AU) that the orbital velocities ($\lesssim 1$ km s^{-1}) are less than the typical radial velocity measurement errors (∼10 km s^{-1}) for faint objects. Such wide separations also strongly suggest that significant mass exchange between the components is unlikely to have occurred (see, e.g., Greenstein 1986; Wood & Oswalt 1992); hence, each star evolves effectively as a single star. Wide orbital separations also facilitate distance determinations, since each component provides an independent estimate. Most of our CPMB nondegenerate companions are cool MS stars whose Hα absorption lines have a negligible gravitational redshift (0.635 km s^{-1} for typical 1 $M_\odot$ star; von Hippel 1996) compared with a typical WD redshift of ∼30 km s^{-1}. Thus, the MS companion provides a relative standard of rest against which the intrinsic gravitational redshift of the WD can be measured. Moreover, the MS star provides the

intrinsic radial velocity of the pair which, taken together with distance and proper motion, yields the complete space motion of the pair.

The MS components are usually brighter (by $m_v \sim 2.5$ mag; see Oswalt et al. 1990) than their WD companions, and the S/N of these spectra are higher than for the WD spectra, particularly in the wavelength range centered around the Hα absorption feature. The majority of the MS components (primarily M dwarfs; see Table 3 for a complete list of spectral types) have well-defined Hα features. Thus, the MS radial velocities and space motions are generally more reliable than the WD gravitational redshift mea-

TABLE 3

COMMON PROPER MOTION BINARY RADIAL VELOCITY DATA

WD Number	Object Name	v_r (km s^{-1})	σ_{v_r} (km s^{-1})	$v_{r,\mathrm{LSR}}$ (km s^{-1})	$\sigma_{v_{r,\mathrm{LSR}}}$ (km s^{-1})	Spectral Type	Run (UT)
0027−545.....	L170-14A	−31.8	5.7	−41.1	5.7	dM3	1991 Nov
0120−024.....	LP 587-53	−8.9	9.9	−15.2	9.9	dM	1991 Nov
0148+641.....	G244-37	−14.9	0.1	−9.3	0.1	dM2	1991 Oct
0150−164.....	G272-B3B	25.2	0.1	14.7	0.1	dM	1992 Jun
0200−170.....	G272-B5A	−22.2	0.1	−33.3	0.1	dG	1991 Nov
0204−306.....	LP 885-23	28.5	6.2	15.8	6.2	dM3	1991 Nov
0251−008.....	BD −1°407	17.0	0.0	5.6	0.0	dG5	1991 Nov
0315−011.....	BD −1°469	2.9	8.9	−10.3	8.9	dG5	1991 Nov
0433+270.....	BD +26°730	−32.3	1.1	−42.1	1.8	dK4	1991 Oct
0443−275.....	LP 891-13	−147.0	5.6	−166.0	5.6	dM4.5e	1991 Nov
0615−591.....	CD −59°1275	−22.1	8.4	−39.5	8.4	dG3	1995 May
0628−020.....	LP 600-43	71.6	0.1	54.1	0.3	dM	1991 Nov
0642−285.....	CD −28°3361	10.9	0.3	−8.8	0.3	dK3	1991 Nov
0726+392.....	LP 207-8	28.4	0.3	22.3	0.3	dM5	1991 Oct
0738−172.....	LP 783-2	−75.4	17.5	−93.9	17.5	dF	1995 May
0820−583.....	L186-120	−78.1	5.9	−94.0	5.9	dM5	1993 Apr
0845−188.....	CD −18°2482	38.3	5.7	22.8	5.7	dK3	1991 Nov
0926−039.....	G161-37	−30.4	14.8	−41.8	14.8	dM5	1993 Apr
1043−034.....	G163-B9A	−49.4	6.8	−55.8	6.8	dF9	1993 Apr
1105−048.....	LP 672-1	26.7	0.1	21.7	0.1	dM6	1995 May
1148+544.....	LP 129-586	−7.8	2.8	−0.2	2.8	dM5	1996 Jun
1211+392.....	LP 216-75	36.5	1.8	43.4	1.8	dM0	1996 Jun
1214+032.....	LP 554-63	−6.6	4.4	−5.0	4.4	sdM3	1996 Jun
1304+227.....	LP 378-537	−39.1	2.0	−30.9	2.0	dK0	1996 Jun
1317−021.....	LP 617-34	−64.2	3.1	−58.2	3.1	dM	1995 May
1327−083.....	G14-57	−1.5	0.9	3.2	0.9	dM5	1992 Jun
1334−160.....	LP 798-13	15.2	0.7	19.0	0.7	dM5e	1992 Jun
1337−023.....	LP 618-90	125.3	11.8	131.8	11.8	dK	1995 May
1348−271.....	LP 856-54	−26.6	36.5	−24.3	36.5	dM3	1995 May
1354+340.....	BD +34°2473	−23.7	0.4	−11.3	0.4	dF	1996 Jun
1541−381.....	LP 480-85	−28.3	6.6	−23.4	6.6	dM3	1993 Apr
1544+005.....	BD +1°13129A	−48.5	3.1	−34.1	3.1	dF8	1993 Apr
1544−377.....	CD −37°6571	−10.6	0.3	−5.4	0.3	dG3	1992 Jun
1550+716.....	LP 42-196	−2.4	10.6	11.6	10.6	dM5+	1996 Jun
1555−089.....	G152-B4B	9.8	8.7	22.7	8.7	dM5	1996 Jun
1620−391.....	CD −38°10983	34.6	0.1	40.4	0.5	dG6	1992 Jun
1623−540.....	L266-195	53.1	0.0	54.2	0.0	dM	1992 Jun
1659−531.....	ϵ^2 Eri	28.2	0.5	30.2	0.5	dF7	1992 Jun
1716+020.....	Wolf 672B	−71.4	6.8	−54.2	6.8	dM5	1993 Apr
1743−132.....	G154-B5A	−106.8	0.3	−92.3	0.3	dM3	1992 Jun
1750+098.....	BD +9°3501	−31.1	0.0	−12.4	0.0	dK4	1993 Apr
1911+135.....	G142-B2B	−35.3	6.7	−16.9	6.7	dM3	1993 Apr
1917−077.....	L923-22	−64.2	1.5	−49.4	1.5	dM5	1995 May
1923+715.....	LP 45-217	−4.7	0.4	9.9	0.4	dM5	1996 Jun
2044−043.....	LP 696-5	−12.0	0.4	0.3	0.4	dM0	1992 Jun
2047+809.....	BD +80°670	−13.2	0.0	−1.3	0.0	sdG7	1991 Oct
2051+095.....	LP 516-12	−20.8	0.3	−6.6	0.3	dM5	1991 Oct
2154−437.....	L427-60	101.9	7.7	101.6	7.7	dM5e	1992 Jun
2249−105.....	LP 761-113	−37.9	3.0	−34.4	3.0	dM3	1996 Jun
2253−081.....	G156-64	−45.0	0.1	−15.2	0.4	dG1	1992 Jun
2318+126.....	LP 522-35	−38.7	0.4	−33.3	0.4	dM5	1991 Oct
2323−241.....	G275-B16B	0.6	24.5	−0.9	24.5	dM	1992 Jun
2341+321.....	LP 347-5	−31.4	1.6	−24.8	1.6	dM5	1991 Oct
2341−164.....	G273-B15A	−19.6	8.1	−21.0	8.1	dM4	1991 Nov
2351−333.....	L577-72	2.9	0.1	3.1	0.1	dM5	1992 Jun
2358+270.....	LP 348-20	−30.4	0.3	−25.6	0.3	dM5	1991 Oct

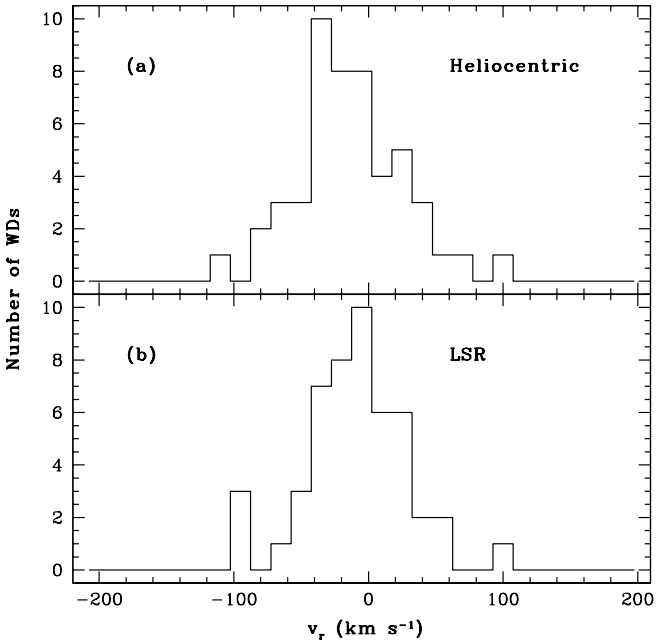

FIG. 1.—(*a*) Heliocentric and (*b*) LSR radial velocity distributions for the sample of CPMBs. Stars without $V-I$ data were omitted from the graph.

surements. For the radial velocity measurements, the wavelength of each MS component's Hα feature was measured relative to the laboratory value of 6562.852 Å. Our measured heliocentric radial velocities (v_r) for 29 MS stars in common were compared with values from Wilson (1963). There was no evidence for any systematic effects, due to instrumentation or the site, that were larger than the measurement error. No radial velocity standards were observed for the 1995 May CTIO and 1996 June Keck observing runs, and hence no adjustments to the measurements were possible for these two runs. Systematic errors in the earlier CTIO data for standard stars proved to be negligible with respect to typical measurement errors, so we were not concerned by the lack of standards for the 1995 May run. As discussed by Reid (1996), the HIRES is located on one of the Nasmyth platforms. This provides an extremely stable wavelength scale, resulting in little chance of instrumental flexure during the 1996 June Keck run.

Figure 1 shows the radial velocity distribution of all CPMBs in our sample corrected to heliocentric (v_r) and local standard of rest ($v_{r,\mathrm{LSR}}$) values, respectively. The mean heliocentric radial velocity for the sample of 56 WDs, as derived from MS companions, is $\langle v_r \rangle = -12.1 \pm 6.1$ km s^{-1}. The mean local standard of rest radial velocity is $\langle v_{r,\mathrm{LSR}} \rangle = -10.8 \pm 6.1$ km s^{-1}. Table 3 lists the individual v_r measurements and uncertainties corrected to heliocentric and LSR velocities. The mean uncertainties in the table represent the scatter typical of three to five independent measurements of the Hα line core. It should be noted that unless otherwise stated, all uncertainties given in this document are standard deviations of the mean ($\sigma_m = \sigma/N^{1/2}$).

4. EINSTEIN REDSHIFTS

Gravitational redshift (v_g) is a consequence of general relativity. Classically, a photon climbing out of a deep gravitational potential well must lose energy. This results in a photon that has a longer wavelength.

In the weak-field regime, the result may be approximated as

$$v_g = \frac{c\Delta\lambda}{\lambda_0} = 0.635 \frac{M/(1\ M_\odot)}{R/(1\ R_\odot)} \text{ km s}^{-1} . \quad (1)$$

This relationship, coupled with effective temperatures and distances, allows the mass of a WD to be determined. Refer to § 5 for the method used in this study to obtain the mass of a WD from equation (1).

Within DA (hydrogen spectrum) WDs, theory predicts that Hα is only slightly affected by pressure shifts, and it exhibits a very sharp non-LTE line core. Thus, Hα is the best choice for investigating the gravitational redshift of a WD (Shipman & Mehan 1976; Grabowski, Madej, & Halenka 1987). Some of the early investigations of WD redshifts measured the Hβ absorption line, as well as Hα. As discussed by Grabowski et al. (1987), the pressure shift (collisional broadening) of the line profile increases with the principal quantum number. Also, Hβ is seldom resolvable in the low-S/N spectra of faint WDs, and in the cases where it is resolved, the results are inconsistent with Hα. Lines of helium and metals are broader still and subject to even larger uncertainties because of pressure shifts (Greenstein & Trimble 1967; Bergeron, Saffer, & Liebert 1992).

The determination of the gravitational redshifts of WDs is, to say the least, a challenging observational problem. The fact that the WD must exhibit a resolvable Hα line core restricts the sample to DA WDs and leaves the question open whether the mean mass of other types of WDs is different (Koester, Schulz, & Wegner 1981; Oke, Weidemann, & Koester 1984). Another complication is that most WDs are very faint for this particular type of study ($V \gtrsim 15$) and, since the gravitational redshifts are small ($\lesssim 1$ Å), the detection of sharp Hα line cores at high S/N requires a tremendous amount of large-telescope time. If the line core is not fully resolved, the derived gravitational redshift is highly dependent on the instrumental resolution because the line wings are asymmetric.

The gravitational redshift (v_g) measurements for 41 WDs (of 56 binaries that had visible Hα features) are displayed in Figure 2. The mean redshift of this distribution is 43.3 ± 4.7 km s^{-1}. Values (v_g) and uncertainties (σ_m) for individual stars are listed in Table 4. It will be shown in the following section that the mass distribution of these 41 stars is bimodal, which is already apparent in the redshift distribution in Figure 2. As shown, there are five stars with redshifts over 100 km s^{-1}. As with the v_r measurements, the uncertainties quoted are derived from the scatter typical of three to five independent measurements of the Hα line core. We employed the same reduction and measurement techniques that were used for the v_r measurements, so there are no systematic effects that would give these five stars a larger redshift than the rest of the stars in the distribution. The bimodality and its implications will be discussed in the following section on the mass distribution.

5. MASS DISTRIBUTION

There are well over 2000 known WDs (McCook & Sion 1999)—yet fewer than 200 WDs have useful mass estimates, and the agreement between different mass estimates for any particular individual WD remains unacceptably poor. The mean WD mass and the shape of the WD mass distribution are strong indicators of the total mass density of WDs in the

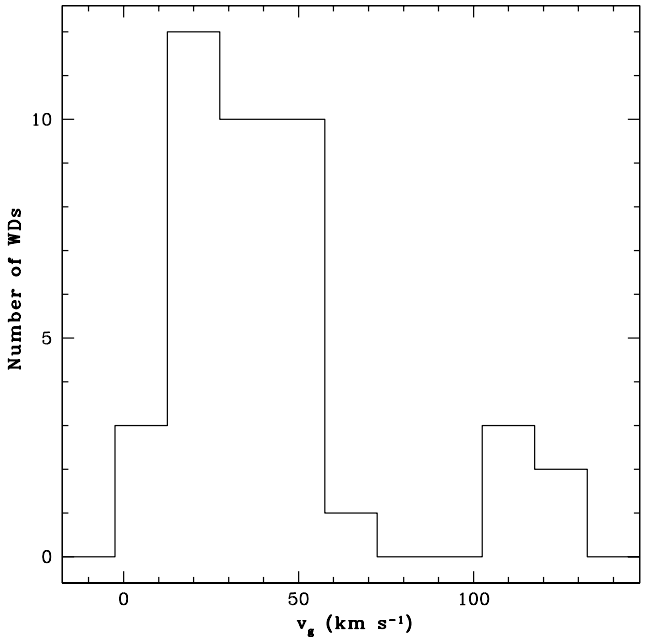

FIG. 2.—WD gravitational redshift distribution. The average is 43.3 ± 4.7 km s^{-1}.

solar neighborhood. A detailed knowledge of the WD mass distribution could provide robust constraints to the initial-final mass relation for WD progenitors, a touchstone for stellar evolutionary models (Finley, Koester, & Basri 1997, hereafter FKB).

Prior works (Koester 1987; Wegner & Reid 1987, 1991; McMahan 1989; Bergeron et al. 1992, hereafter BSL; Bergeron et al. 1995, hereafter BLF; Reid 1996; Bergeron, Ruiz, & Leggett 1997, hereafter BRL; Giovannini et al. 1998) have established the average WD mass to be in the 0.50 $M_\odot < M < 0.70$ $M_\odot$ range. The key connection between gravitational redshift measurements and WD mass estimates is the theoretical mass-radius relationship (see Vennes et al. 1995; Wood 1995). The masses reported in this study have been obtained assuming the mass-radius relation implicit in Wood's (1995) evolutionary models, which were used to generate a grid of models for DA WDs ranging in mass from 0.2 to 1.2 $M_\odot$, in 0.1 $M_\odot$ increments. These models have relatively thick surface hydrogen layers ($10^{-4} M_*$) on top of a helium layer ($10^{-2} M_*$), surrounding a carbon core. Wood's models are also computed for a carbon-oxygen core composition, but there is no difference in the mass of the WD imposed by the core composition as long as $\mu_e = 2$, which is the case for both C and O core compositions. Thus, our choice of model core composition is arbitrary. The use of the thick envelope models is recommended by FKB to maintain consistency between planetary nebulae and WD birth rates. However, we find the measurement errors are larger ($\gtrsim 0.05$ $M_\odot$) than any difference imposed by the models (< 0.01 $M_\odot$; Wood 1992). Furthermore, Reid (1996) showed that spectroscopic masses computed using thick hydrogen envelopes are in much better agreement with gravitational redshift results than the thin hydrogen envelope results obtained by BLF.

To determine a theoretical mass from the model mass-radius relation, the theoretical v_g was derived for each model mass. A fourth-order polynomial was fitted to the theoretical v_g-mass curve at the WD's temperature. From the measured v_g, the mass was found for each WD at its $T_{\rm eff}$, and the mean v_g uncertainty was propagated accordingly to obtain the final uncertainty in mass.

Figure 3 shows three examples of theoretical gravitational redshift v_g (in kilometers per second) versus model mass (in solar units) at temperatures $T_{\rm eff} = 5000$, 10,000, and 20,000 K. This figure shows that the temperature has very little effect on the estimated mass of the WD (± 0.01 $M_\odot$)—especially in the low-temperature regime probed by our sample. Nevertheless, we used the curve corresponding to the best temperature estimate of the WD to determine its mass from the model sequences.

The individual temperatures of the WDs were determined primarily from $V-I$ color determined in a parallel $BVRI$ photometry effort (see Oswalt et al. 1990; Smith 1997). Where our photometry was not available, $T_{\rm eff}$ estimates were taken from the literature as noted in Table 4. In the case where more than one value for the temperature of the WD was found, the most recent literature value was used.

The mass distribution for the 41 WDs shown in Figure 4 has a mean mass of $\langle M \rangle = 0.68 \pm 0.04$ $M_\odot$. Table 4 lists the individual masses and their uncertainties. Within the limits of the mean uncertainties quoted, this mass distribution has a higher mean than most studies as shown in Table 5. For example, our mean mass is more than 2 σ_m larger than the mean mass reported by studies of mostly hotter WDs, such as those of BSL, Reid (1996), and FKB. On the other hand, our mean WD mass is in good accord with studies such as that of BRL, where $T_{\rm eff} \lesssim 12{,}000$ K. Nevertheless, within our sample there is no statistically significant relationship between mass and either $V-I$ or $T_{\rm eff}$ (see Fig. 5). What then accounts for the different mean masses among these samples?

To compare with the prior studies of BLF and Bragaglia, Renzini, & Bergeron (1995, hereafter BRB), we split our

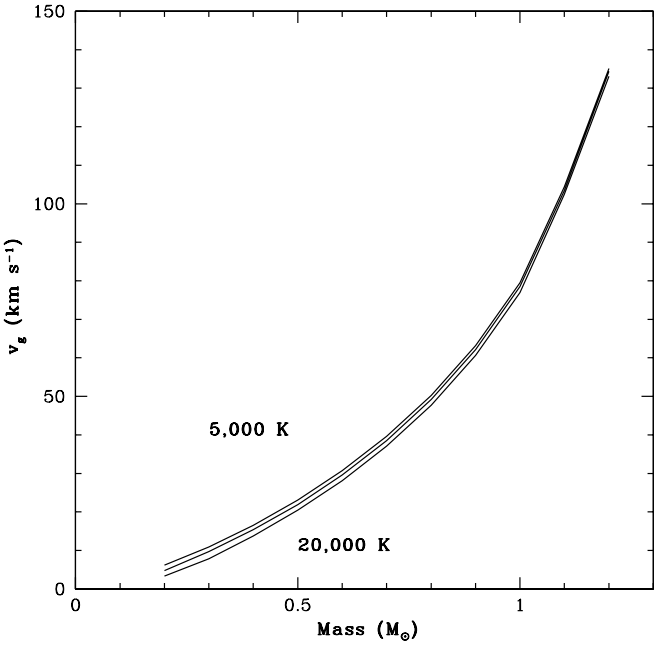

FIG. 3.—Example of three v_g vs. M relationships. Values are from WDEC models (Wood 1995) at three effective temperatures of 5000 K (*left*), 10,000 K, and 20,000 K (*right*). Clearly there is very little dependence on the temperature for WDs with masses 0.2–1.2 $M_\odot$. The difference between any two temperatures introduces, at most, a difference in estimated mass of ~ 0.01 $M_\odot$.

TABLE 4

COMMON PROPER MOTION BINARY REDSHIFT AND MASS DATA

WD Number	Object Name	$V-I$	$T_{\rm eff}$ (K)	$T_{\rm eff}$ Ref.	v_g (km s^{-1})	σ_{v_g} (km s^{-1})	M ($M_\odot$)	σ_M ($M_\odot$)	Age (Gyr)	Spectral Type
0027−549.....	L170-14B	1.035	4866	1	44.1	5.6	0.75	0.05	6.24	DA
0120−024.....	LP 587-53	0.704	6037	1	39.1	9.7	0.66	0.10	2.35	DA
0148+641.....	G244-36	0.300	8516	1	49.7	0.7	0.81	0.01	0.95	DA6
0204−306.....	LP 885-22[a]	0.786	5709	1	50.9	6.8	0.81	0.06	2.93	DA
0251−008.....	LP 591-117	0.615[b]	6453	1	20.8	0.3	0.49	0.01	1.98	DA
0315−011.....	LP 592-80	...	7030	2	30.3	5.8	0.60	0.07	1.58	DA
0433+270.....	LP 358-525	0.820	5575	1	110.6	1.3	1.12	0.01	3.43	DA[c]
0628−020.....	LP 600-42	0.940	5161	1	31.1	0.5	0.62	0.01	5.14	DA
0642−285.....	LP 895-41	0.235	9050	1	58.3	1.9	0.78	0.05	0.81	DA
0738−172.....	LP 783-3	0.346	8156	1	107.5	14.0	1.11	0.05	1.07	DZAQ6
0820−585.....	L186-119	0.270	8762	1	103.6	8.3	1.10	0.03	0.88	DA
1105−048.....	LP 672-1	−0.180	17081	1	23.8	5.1	0.51	0.08	0.13	DA3
1211+392.....	LP 216-74	−0.211	19595	1	23.7	2.3	0.53	0.03	0.08	DA3
1304+227.....	LP 378-537	...	...	5	9.1	2.8	0.29	0.05	...	DA
1317−021.....	LP 617-35	1.192	4389	1	21.3	10.5	0.46	0.14	7.74	DA
1327−083.....	G14-58	−0.153	15474	1	21.8	4.4	0.50	0.06	0.19	DA4
1334−160.....	LP 798-13	−0.055	12271	1	45.0	2.2	0.77	0.02	0.37	DA
1337−023.....	LP 618-89[d]	1.852	3500[b]	1	34.3	16.9	0.63	0.19	10.00	DA
1348−273.....	LP 856-53	0.380	7901	1	27.0	8.2	0.53	0.09	1.16	DA6
1354+340.....	G165-B5B	−0.066	12500	1	17.8	4.1	0.43	0.06	0.35	DA
1541−381.....	LP 480-85[d]	1.742	4060	1	55.2	0.9	0.85	0.01	...	DA
1544+009.....	BD +0°13129	0.386	7859	1	8.8	1.4	0.29	0.03	1.18	DAB
1544−377.....	L481-60	0.800[e]	5654	1	27.3	0.7	0.58	0.01	3.10	DA7
1550+716.....	LP 42-195	...	...	5	48.3	7.7	0.78	0.07	...	DA
1555−089.....	G152-B4B	−0.103	13438	1	49.1	4.2	0.80	0.04	0.29	DA5
1620−391.....	CD −38°10980	−0.277	26667	1	33.9	0.4	0.65	0.01	0.02	DA2
1623−540.....	L266-196	−0.155	15579	1	49.8	5.2	0.80	0.04	0.18	DAe
1659−531.....	L268-92	...	11800	3	39.0	0.6	0.71	0.08	0.41	DA4
1716+020.....	G19-20	−0.011	11354	1	30.9	5.0	0.60	0.06	0.45	DA4
1743−132.....	G154-B5B	0.285	8639	1	27.4	1.1	0.58	0.01	0.92	DA
1750+098.....	G140-B1B	0.178	9527	1	126.6	9.0	1.17	0.02	0.71	DA[f]
1911+135.....	G142-B2A[d]	−0.074	12700	1	22.4	2.5	0.50	0.04	0.33	DA
2044−043.....	LP 696-4	0.275	8721	1	22.2	7.6	0.47	0.10	0.90	DA5
2048+809.....	LP 25-436	0.700[g]	6056	1	23.8	2.4	0.53	0.03	2.33	DA7
2051+095.....	LP 516-13	−0.149	15263	1	10.7	0.3	0.32	0.01	0.20	DA
2249−105.....	LP 761-114[d]	1.750	4020	1	45.6	11.9	0.75	0.10	...	DA
2253−081.....	G156-64	0.640	6336	1	45.1	0.3	0.77	0.01	2.07	DA8
2323−241.....	G275-B16A	0.582	6628	1	132.0	1.1	1.19	0.01	1.84	DA
2341+322.....	LP 347-4	...	13580	4	33.4	1.2	0.65	0.01	0.28	DA4
2351−335.....	L577-71	0.560	6750	1	31.2	7.4	0.58	0.08	1.76	DA5
2358+270.....	LP 348-19	0.249	8934	1	41.3	11.0	0.71	0.12	0.84	DA

[a] Reid 1996 cited as possible nonphysical pair.
[b] Smith 1997 noted possible problem with photometry.
[c] Noted in McCook & Sion 1999 as spectral type DC8.
[d] Smith 1997 noted as possibly having an unresolved companion based on JHK photometry.
[e] V and $V-I$ photometry from (4).
[f] Noted in McCook & Sion 1999 as spectral type DC5.
[g] V and $V-I$ photometry from (3).

REFERENCES.—(1) $T_{\rm eff}$ from $V-I$ measured by Smith 1997; (2) Barker 1993; (3) Provencal et al. 1998; (4) Giovannini et al. 1998; (5) no photometry and no temperature found in literature.

sample of WDs into two subgroups: one with $T_{\rm eff} \lesssim 12{,}000$ K and one with $T_{\rm eff} \gtrsim 12{,}000$ K. In the former group, $\langle M \rangle = 0.72 \pm 0.04\ M_\odot$ for 28 WDs, and in the latter group, $\langle M \rangle = 0.59 \pm 0.05\ M_\odot$ for 11 WDs. As with BLF and BRB, it appears in our sample that WDs with $T_{\rm eff} <$ 12,000 K are on average more massive than hotter WDs, but this is entirely due to a group of five massive WDs that apparently form a second peak at $\sim 1.2\ M_\odot$ (see Figs. 4 and 5). Statistically, this peak is significant; a simple Wilcoxon test reveals a 0.1% probability that the two groups of WDs (low- and high-mass peaks) originate from the same parent population.

Table 5 is a compilation of the available studies of the WD mass distribution. In general, there seems to be a trend toward higher average masses for deeper and fainter samples. There also appears to be a consistent asymmetry toward higher masses about the mean WD mass (see Koester, Schulz, & Weidemann 1979; Weidemann & Koester 1984; McMahan 1989; BSL, BLF; BRB; BRL; FKB; Giovannini et al. 1998). We hypothesize that there is a high-mass sequence above 1 $M_\odot$ in our sample, i.e., that our mass distribution is bimodal.

Most of the mass distributions in Table 5 exhibit a secondary "peak" in the low- and/or high-mass tail of the

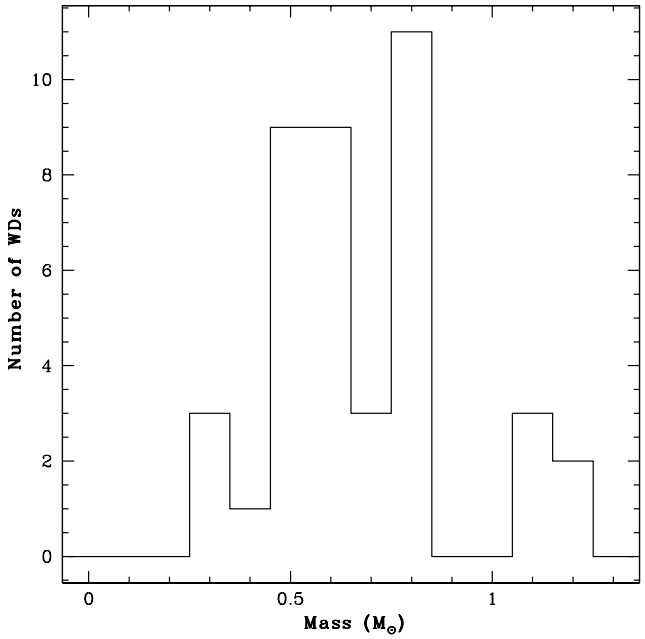

FIG. 4.—Mass distribution for 41 WDs. The sample's mean mass is $\langle M \rangle = 0.68 \pm 0.04\ M_\odot$. The distribution appears bimodal, with one peak at a mean of $0.61 \pm 0.03\ M_\odot$ and a high-mass peak at a mean of $1.12 \pm 0.03\ M_\odot$.

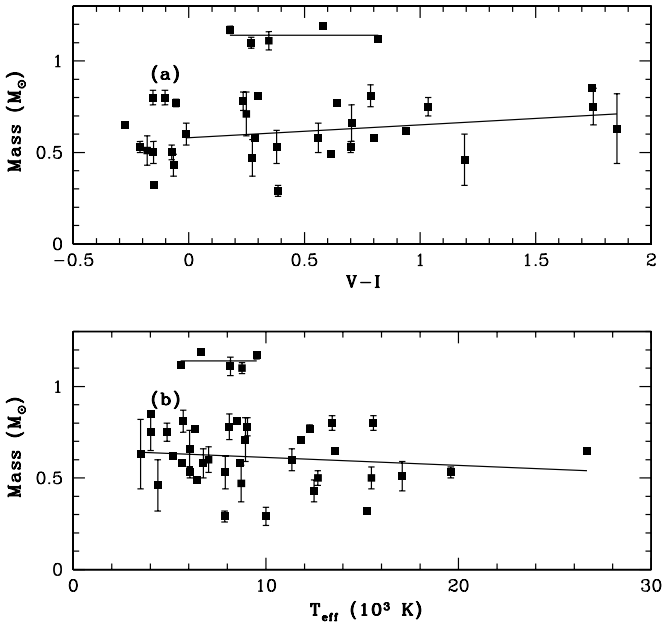

FIG. 5.—(*a*) M vs. $V-I$ color plot and (*b*) M vs. $T_{\rm eff}$ plot. Though there appears to be a trend in both plots, the slopes and regression values for both lines are statistically insignificant.

distribution. BSL report a narrow WD mass distribution with high- and low-mass secondary peaks on either side. Their highest mass WD in a sample of 129 WDs is GD 50, with an estimated mass of 1.3 $M_\odot$. The BLF sample has three of 35 WDs between 0.9 and 1.1 $M_\odot$. This is a similar percentage to our sample, where we have five WDs with masses between 1.0 and 1.2 $M_\odot$. Schmidt et al. (1992) called attention to two massive WDs: PG 0136+251 ($M_{\rm WD} = 1.20 \pm 0.02\ M_\odot$) and PG 1658+441 ($M_{\rm WD} = 1.31 \pm 0.02\ M_\odot$), both of which are more massive than any in our sample. These two stars are believed to have larger than normal magnetic fields for WDs. According to Sion &

TABLE 5

MEAN MASS COMPARISON FOR SEVERAL STUDIES

Study Group	No. of WDs	M ($M_\odot$)	σ_M ($M_\odot$)	Model[a] Used	Avg. $T_{\rm eff}$ (K)	Notes[b]	Ref.
SEA.....	41	0.68	0.22	W95	~10,000	$\sigma_m = 0.04\ M_\odot$	1
	28	0.72	0.23	W95	$\lesssim$12,000	$\sigma_m = 0.04\ M_\odot$	1
SEA.....	13	0.59	0.16	W95	$\gtrsim$12,000	$\sigma_m = 0.05\ M_\odot$	1
	60	0.660	0.190	W95	$\lesssim$12,000		
FKB	174	0.570	0.060	W92, W95	$\gtrsim$25,000	σ via Gaussian fit	
R96	53	0.581	0.078	W95	...	Median mass	2
BLF.....	22	0.601	0.148	W90	...	Unw	
	22	0.583	...	W90	...	w; $\sigma_m = 0.006\ M_\odot$	
	31	0.593	0.134	W90	$\gtrsim$12,000		
	12	0.710	0.111	W90	$\lesssim$12,000		
BRB	46	0.587	0.166	W90, W92	$\gtrsim$12,000		
	42	0.609	0.157	W90, W92	$\gtrsim$12,000	Four omitted by BRB	
BSL.....	129	0.562	0.137	W90	$\gtrsim$15,000		
WR91.....	35	0.630	...	HS	...	$\sigma_m = 0.03\ M_\odot$	3
KR	122	0.580	0.100	HS	...		4
McM	52	0.571	0.188	W90	...		5
	52	0.480	...	HS	...	w; $\sigma_m = 0.014\ M_\odot$	5
	52	0.546	0.192	HS	...	Unw	5
K87	9	0.580	0.100	HS	...		6
WK	70	0.603	0.133	W90	...		7
	70	0.580	0.130	HS	...		7
G82	70	0.620	0.130	HS	...		8
KSW	122	0.602	...	HS	...	$\sigma_m = 0.093\ M_\odot$	9

[a] (W90) Wood 1990; (W92) Wood 1992; (W95) Wood 1995; (HS) Hamada & Salpeter 1961.

[b] (Unw) unweighted mean mass; (w) weighted mean mass—refer to reference for weighting methods.

REFERENCES.—(1) Silvestri et al. 2000, this study; (2) Reid 1996; (3) Wegner & Reid 1991; (4) Koester & Reimers 1989; (5) McMahan 1989; (6) Koester 1987; (7) Weidemann & Koester 1984; (8) Greenstein 1982; (9) Koester et al. 1979.

Oswalt (1988), Schmidt et al. (1992), and Anselowitz et al. (1999), magnetic WDs appear to be more massive than their nonmagnetic counterparts. There is no evidence of large magnetic fields in the most massive WDs in our sample; no Zeeman splitting was observed in the line profiles, and no references to polarization in these objects are reported in the literature.

If we omit the five high-mass WDs from our distribution we obtain a mean mass of $0.61 \pm 0.03\ M_{\odot}$, which, within errors, is equivalent to studies such as those by McMahan (1989), BLF, BRB, and Reid (1996). This would imply that samples that extend to cooler temperatures, on average, appear more massive because cool WDs are intrinsically more numerous and, therefore, contain a larger number of massive WDs. Presumably the percentage of high-mass WDs extends to hotter samples. As determined by FKB, a mass distribution is highly sample dependent.

One explanation for the appearance of high-mass WDs is unresolved companions. As found by BSL and BRL, several WDs in their samples are believed to have unresolved companions. We suspect three such WDs in our sample (see Table 4) originally suggested by Smith (1997). If the unseen companion is a high-mass, cool degenerate (DA) and less luminous than the WD seen, this effect could easily go unnoticed during the reduction process yet still affect the WD line core. The additional line core from the unseen companion may be indistinguishable from a single WD Hα profile, but the centroid would be redshifted in a low-S/N spectrum. Such unresolved pairs would still need to have large enough semimajor axes for the relative orbital motion to be negligible. Alternatively, the reason for the existence of high-mass WDs in older samples could simply be that older WDs were formed from more massive progenitors (Wood 1992). This scenario requires a star formation rate that forms high-mass stars early in the history of the Galactic disk. A better understanding of the early history of the Galaxy and initial-final mass relation would be necessary to strengthen this hypothesis.

At present, the most attractive explanation for the high-mass peak is prior mass transfer from an unresolved MS companion or mergers of WDs that have produced some unusually high- (or low-) mass WDs (Iben & Tutukov 1984). Note that the second mass peak in Figure 4 is suspiciously close to twice the mean mass of most WDs. The high-mass peak in our study could be the result of double-degenerate mergers. If the original separation of the two stars is such that the primary becomes enveloped in the evolving secondary's atmosphere, friction would degrade the orbit until the two stars merge, thereby creating the high-mass WDs seen in cooler samples. Cooler and, therefore, older WDs with close companions have had adequate time for both stars to evolve off the MS. As binaries are common, samples of single WDs, as opposed to our sample of known binaries, are likely to be significantly affected by unresolved companions.

It becomes progressively more difficult to estimate masses for WDs cooler than about 10,000 K (Koester et al. 1979). In such stars, the Hα line becomes weak and there are substantial differences in models. As discussed by BSL, BLF, and BRL, large amounts of helium can be brought to the surface by convection at $T_{\rm eff}$ between 12,000 and 6,000 K. This effect broadens the line profile through van der Waals forces induced by neutral helium in the WD's atmosphere. In the low-S/N regime of these cool, faint objects, the broadening of the line because of helium increases the uncertainty in the location of the Hα line core, making it difficult to distinguish between pressure effects from the increase of helium at the surface and an actual increased surface gravity because of high mass. However, BRL found mixed H and He atmosphere WDs to be a relatively rare occurrence. This effect is difficult to distinguish from the effects of an unseen degenerate (non-DA) companion, whose spectrum would dilute the Hα line profile of the DA WD (see BRL's discussion of G141-2). The problem of contamination by an unresolved companion is currently one of the largest uncertainties in determining the masses of cool WDs. Fortunately, it is less a problem in our wide pairs than in single field WDs because close tertiary companions are much less common (see Poveda et al. 1994) than close binary companions.

Fontaine & Wesemael (1987), Sion & Oswalt (1988), Bergeron et al. (1990), BRL, and Hansen (1999) discuss the observed ratio of DA to non-DA WDs as a function of temperature. Bergeron et al. (1990) found that the ratio of DA to non-DA single WDs hotter than $T_{\rm eff} \sim 12{,}000$ K is 6:1 compared with 2:1 for $7500\ {\rm K} < T_{\rm eff} < 12{,}000$ K. This would be expected if mixing occurs between the heavier underlying helium layer and the lighter surface hydrogen layer as a WD cools. Because the majority of our WDs are cooler than 12,000 K, it is important to emphasize that our apparent high mean WD mass below this temperature may be due, in part, to convectively mixed helium in the atmosphere rather than an increased surface gravity. The line broadening due to the presence of helium may be misinterpreted as the effect of high mass. WDs may still have observable Hα features, as only a small amount of hydrogen ($\sim 10^{-14}\ M_{\odot}$ in the atmosphere of the WD) is required to produce an observable Hα feature.

Finally, we must address the existence of three WDs in our sample with masses less than $0.46\ M_{\odot}$. At present, the Galaxy is not old enough for single WDs with a mass less than $0.46\ M_{\odot}$ (FKB) to have formed, so common-envelope evolution is required to produce WDs with these low masses. As discussed earlier, a plausible explanation is close binary evolution. This seems to be the case for many low-mass WDs, as discussed by Marsh, Dhillon, & Duck (1995). It could also be argued that low-mass WDs could be more prevalent in samples of predominantly cool WDs as a result, in part, of differential cooling. As noted by FKB, the only low-mass star in their sample was found at a temperature below 30,000 K. FKB argue that the increased presence of low-mass stars in cool samples results from a significant amount of contraction while these stars cool. Rapid cooling of initially hot low-mass WDs would prevent them from being detected by surveys of hotter WDs. This would increase the frequency with which they are detected by cool samples like ours. All of the low-mass objects in BSL have temperatures below 30,000 K as well. Two of the low-mass WDs in our sample lie below 20,000 K. The third star has no photometry and, subsequently, no temperature estimate. However, our current sample provides no strong test of this scenario.

Table 6 lists our individual mass estimates compared with those reported by other studies. Although mean masses agree rather well, the individual WD masses reported in the literature often are not consistent with ours or with each other. It is particularly frustrating that the measurement uncertainties in the individual methods are frequently

TABLE 6

MASS COMPARISON FOR CPMBS

WD Number	SEA[a]	WR91[b]	R96[c]	KSW[d]	K87[e]	BLF	BSL	BRB	W89[f]
0148+641.....	0.81	...	0.67	...	...	...	...	...	...
0251−008.....	0.49	0.50	0.62	...	...	...	...	...	...
0628−020.....	0.62	...	0.53	...	...	...	...	...	...
0642−285.....	0.78	...	0.54	...	...	...	...	...	...
1105−048.....	0.51	...	...	0.54	0.45	...	0.49	...	0.44
1327−083.....	0.50	...	...	0.59	0.52	0.53	...	0.50	...
1334−160.....	0.77	0.82	...	...	0.79	0.54	0.54	...	...
1348−271.....	0.53	...	...	...	0.49	...	...	...	...
1354+340.....	0.43	0.47	...	0.59	...	0.49	...	...	...
1544+005.....	0.29	...	...	0.15	...	...	...	...	...
1544−377.....	0.58	...	...	0.21	0.56	...	...	...	...
1555−089.....	0.80	0.66	...	0.39	...	0.66	...	0.52	...
1620−391.....	0.65	...	...	0.27	0.67	...	...	0.66	0.69
1659−531.....	0.71	...	...	0.55	0.58	...	...	...	...
1716+020.....	0.60	...	0.59	0.51	0.47	...	...	...	...
1743−132.....	0.58	...	0.52	0.32	...	0.52	...	...	...
1750+098.....	1.17	0.60	...	...	...	0.43	...	...	...
1911+135.....	0.50	0.73	0.61	0.53	...	0.56	0.49	...	...
2044−043.....	0.47	0.42	0.43	...	...	0.44	...	...	...
2048+809.....	0.53	0.64	0.64	...	...	0.64	...	...	...
2253−081.....	0.77	0.54	0.40	...	...	0.55	...	...	...
2341+321.....	0.65	...	0.61	0.55	...	...	...	...	...
2351−333.....	0.58	0.54	...	...	...	0.55	...	...	...
2358+270.....	0.71	...	...	...	...	0.76	...	...	...

NOTE.—BRL and FKB have no stars in common with our sample. Units are solar masses.

[a] Silvestri et al. 2000, this study.

[b] Wegner & Reid 1991.

[c] Reid 1996.

[d] Koester et al. 1979.

[e] Koester 1987.

[f] Wegner 1989.

unknown, making it impossible to identify the most reliable estimates. Thus, we have attempted to remove the potential effects of measurement technique, instrumental resolution, and sky contamination— all of which can profoundly affect v_g and v_r measurements. Moreover, we report objectively determined uncertainties in our mass determinations for better comparison to future work.

6. KINEMATICS: UVW SPACE MOTIONS

The gravitational forces acting on a star are determined by the gross structure of the Galaxy, which does not change considerably over long timescales (Binney & Tremaine 1987). Thus, the present kinematic properties of any group of stars reflect its dynamical history and, by inference, the dynamical characteristics and evolution of the Galaxy itself (Mihalas & Binney 1968).

Most kinematic studies of WDs have, out of necessity, used a null radial velocity assumption ($v_r = 0$) to compute space motions (Sion & Liebert 1977; Sion & Oswalt 1988; Sion et al. 1988; Anselowitz et al. 1999). This has been useful in comparing the overall kinematic properties of distinct subgroups of WDs, but it uses only two-thirds of the motion.

Using proper motions and position angles from the literature, photometric and trigonometric parallaxes (assuming no error in trigonometric parallaxes, typical $\sigma_{M_v} \sim 0.3$) from Smith (1997 and sources therein), and radial velocities determined in this study, we computed the total space motion (T), tangential velocity (v_t), and the vector components (U, V, W) relative to the LSR, using a modified procedure similar to that used by Sion et al. (1988). U is positive in the direction of the Galactic anticenter, V is positive in the direction of Galactic rotation, and W is positive in the direction of the north Galactic pole.

Total space velocity is defined by

$$T = (U^2 + V^2 + W^2)^{1/2} \quad (2)$$

or, in terms of radial and tangential velocity,

$$T = (v_r^2 + v_t^2)^{1/2} \quad (3)$$

with $v_t = 4.74\mu d$ (in kilometers per second), where μ is the proper motion (in arcseconds per year) and d is the distance (in parsecs).

The values in Table 7 are WD number (col. [1]), the heliocentric radial velocity, the error in v_r, U, σ_U, V, σ_V, W, σ_W (components of the space velocity), the tangential velocity, σ_{v_t}, total space velocity, and σ_T (cols. [2]–[13]; km s^{-1}). Column (14) is the reduced proper motion of the WD, which is defined by

$$H_v = 5 \log \mu + m_v + 5 \quad (4)$$

and is equivalent to

$$H_v = M_v + 5 \log v_t - 3.38 \, . \quad (5)$$

Column (15) is the error in H_v, and finally, column (16) lists the spectral type of the WD. The mean of each space motion component for the entire sample and its corresponding dispersion ($\sigma_U, \sigma_V, \sigma_W$) are given in Table 8.

The velocity dispersion of our sample of WDs is similar to, though slightly larger than, that of the single late-type

TABLE 7

COMMON PROPER MOTION BINARY SPACE-MOTION DATA

WD Number (1)	v_r (2)	σ_{v_r} (3)	U (4)	σ_U (5)	V (6)	σ_V (7)	W (8)	σ_W (9)	v_t (10)	σ_{v_t} (11)	T (12)	σ_T (13)	H_v (14)	σ_{H_v} (15)	Spectral Type (16)
0027−549.....	−31.8	9.9	−5.3	4.0	0.1	6.6	28.8	6.2	29.3	12.0	43.2	10.9	23.5	1.1	DA
0120−024.....	−8.9	17.2	47.9	5.3	−35.4	8.4	10.7	14.1	60.5	10.9	61.1	11.0	23.1	1.0	DC
0148+641.....	−14.9	0.3	10.3	0.1	−33.3	0.2	−16.2	0.1	38.4	0.3	41.2	0.3	21.1	0.5	DA6
0150−164.....	25.2	0.3	2.8	0.1	−50.4	0.1	−38.6	0.2	63.6	0.3	68.4	0.3	19.8	0.5	DBA
0200−171.....	−22.2	0.3	−1.6	0.1	−17.0	0.1	12.4	0.2	21.1	0.3	30.6	0.3	20.1	0.5	DA
0204−306.....	28.5	10.7	42.5	5.0	−25.0	6.0	−28.1	7.3	56.8	9.3	63.5	9.6	23.5	1.0	DA
0251−008.....	17.0	0.0	81.9	0.0	−38.1	0.0	29.7	0.0	95.1	0.0	96.6	0.0	21.9	0.0	DA
0433+270.....	−32.3	1.8	−21.7	1.4	−36.5	1.0	8.3	0.7	43.3	1.9	54.0	1.9	23.1	0.3	DA[a]
0615−591.....	−22.1	14.5	−2.6	8.8	−7.0	9.9	−20.2	5.9	21.5	12.9	30.8	13.7	18.9	1.1	DB4
0628−020.....	71.6	0.3	65.4	0.2	−56.3	0.1	−27.6	0.1	90.6	0.3	115.5	0.3	25.4	0.5	DA
0726+392.....	28.4	0.5	12.8	0.4	−54.6	0.3	−11.6	0.2	57.3	0.6	64.0	0.6	19.6	0.2	DA
0738−172.....	−75.4	30.3	−69.4	23.4	15.1	14.9	21.8	12.3	74.3	32.7	105.9	31.5	23.1	1.5	DZQ6
0820−585.....	−78.1	10.3	51.8	5.7	75.9	7.0	−25.9	4.9	95.5	11.4	123.3	11.0	22.9	1.1	DA
0845−188.....	38.3	9.9	65.5	6.4	−32.0	5.0	−29.1	5.7	78.5	9.3	87.4	9.4	21.2	1.0	DB4
0926−039.....	−30.4	25.7	42.7	14.0	9.9	12.3	−63.8	17.7	77.4	29.1	83.1	28.6	20.9	1.5	DA
1043−034.....	−49.4	11.8	−4.6	3.5	20.1	5.8	−42.2	9.7	47.0	18.0	68.2	15.1	24.5	1.3	DAB
1105−048.....	26.7	0.3	−11.3	0.1	−63.9	0.1	−12.9	0.2	66.2	0.3	71.4	0.3	20.3	0.6	DA3
1148+544.....	−7.8	4.8	81.8	1.9	−60.7	3.2	−30.5	3.0	106.3	3.9	106.6	3.9	22.4	0.6	DA5
1211+392.....	36.5	3.1	100.8	1.0	−2.1	1.9	8.6	2.3	101.2	1.4	107.5	1.7	20.9	0.1	DA3
1214+032.....	−6.6	7.6	46.2	0.7	−14.5	3.8	−11.6	6.6	49.8	2.9	50.2	3.1	22.7	0.5	DA
1317−021.....	−64.2	5.4	0.5	1.6	−10.3	2.6	−84.0	4.4	84.7	8.8	106.3	7.7	25.5	0.9	DC
1327−083.....	−1.5	1.6	58.4	0.6	−88.4	0.8	−17.1	1.3	107.3	1.3	107.3	1.3	21.3	0.1	DA4
1334−160.....	15.2	1.1	17.7	0.4	−44.6	0.6	0.3	0.9	47.9	1.1	50.3	1.1	20.1	0.0	DA
1348−271.....	−26.6	63.2	7.6	26.6	−6.4	34.7	−46.3	45.6	47.3	89.0	54.3	83.5	21.7	1.9	DA6
1354+340.....	−23.7	0.7	54.6	0.3	−48.4	0.4	−16.1	0.5	74.7	0.6	78.4	0.6	21.0	0.2	DA
1541−381.....	−28.3	11.4	33.9	7.3	−1.0	6.7	−13.6	5.7	36.5	10.4	46.2	10.8	27.8	1.0	DA
1544+009.....	−48.5	5.3	56.5	3.8	−22.9	2.5	−24.7	2.7	65.8	5.4	81.7	5.4	20.4	0.7	DAB
1544−377.....	−10.6	0.5	23.9	0.3	−28.5	0.3	−2.6	0.2	37.3	0.5	38.7	0.5	20.4	0.3	DA7
1555−089.....	9.8	15.0	−7.6	11.1	−32.6	7.1	−9.0	7.2	34.7	14.3	36.0	14.4	19.4	1.2	DA5
1620−391.....	34.6	0.3	−25.0	0.2	−20.4	0.2	−5.9	0.1	32.8	0.3	47.7	0.3	19.1	0.6	DA2
1623−540.....	53.1	0.0	−33.2	0.0	−30.1	0.0	−1.9	0.0	44.9	0.0	69.5	0.0	21.1	0.0	DAe
1659−531.....	28.2	0.8	−21.5	0.5	−28.2	0.5	−18.9	0.3	40.2	0.8	49.1	0.8	19.8	0.1	DA4
1716+020.....	−71.4	11.8	54.5	10.1	−108.3	5.4	1.8	2.9	121.3	12.1	140.7	12.0	22.5	1.1	DA4
1743−132.....	−106.8	0.5	115.7	0.4	−29.7	0.2	−21.5	0.1	121.3	0.5	161.6	0.5	23.9	0.3	DA
1750+098.....	−31.1	0.0	20.7	0.0	−46.4	0.0	−30.0	0.0	59.0	0.0	66.7	0.0	21.2	0.0	DC5
1911+135.....	−35.3	11.6	25.5	9.4	−48.1	5.5	−15.4	3.8	56.6	11.7	66.7	11.6	20.7	1.1	DA
1917−077.....	−64.2	2.6	57.8	2.1	−50.6	1.2	3.0	0.9	76.9	2.9	100.2	2.8	22.2	0.5	DBZ
1923+715.....	−4.7	0.7	15.9	0.4	−11.6	0.5	4.3	0.3	20.2	0.7	20.7	0.7	20.2	0.2	DA
2044−043.....	−12.0	0.7	−29.9	0.5	−71.1	0.3	−11.1	0.4	78.0	0.7	78.9	0.7	22.2	0.2	DA5
2048+809.....	−13.2	0.0	9.8	0.0	−27.2	0.0	−4.1	0.0	29.1	0.0	32.0	0.0	20.9	2.3	DA7
2051+095.....	−20.8	0.5	47.8	0.3	11.9	0.2	33.3	0.3	59.5	0.4	63.0	0.4	20.2	0.4	DA
2154−437.....	101.9	13.3	−48.2	6.3	−48.9	8.3	−96.2	8.4	118.2	14.9	156.0	14.3	22.5	1.2	DB3
2249−105.....	−37.9	5.2	19.2	1.5	−32.5	2.6	23.2	4.3	44.3	5.5	58.3	5.4	28.2	0.7	DA
2253−081.....	−45.0	0.3	96.6	0.1	−61.4	0.1	−8.7	0.2	114.8	0.1	123.3	0.2	24.4	0.8	DA8
2318+126.....	−38.7	0.6	88.7	0.1	−51.7	0.3	9.2	0.5	103.1	0.3	110.1	0.4	21.3	0.5	DA
2323−241.....	0.6	42.5	4.8	10.3	−15.7	23.0	−7.3	34.2	18.0	47.6	18.0	47.6	20.3	1.7	DA
2341+322.....	−31.4	2.8	−17.8	0.8	−32.3	1.6	8.7	2.1	37.9	2.7	49.3	2.7	20.2	0.4	DA4
2341−164.....	−19.6	14.0	−23.5	2.3	−39.6	7.2	9.8	11.7	47.2	11.9	51.1	12.2	20.9	1.1	DA
2351−335.....	2.9	0.3	−20.5	0.1	−26.8	0.2	−3.0	0.2	33.8	0.2	33.9	0.2	21.4	0.7	DA5
2358+270.....	−30.4	0.5	34.6	0.1	−61.4	0.3	−8.9	0.4	71.1	0.4	77.2	0.4	22.0	0.4	DA

[a] Noted in McCook & Sion 1999 as spectral type DC8.

MS stars studied by Upgren (1972, 1978), Wielen (1974), and Weistrop (1977). Old stars, such as the MS companions in our sample, tend to have larger velocity dispersions than young stars. This is the cumulative effect of encounters with molecular clouds and spiral arms, star-star interactions, and possibly the evolution of disk height with time. Typically, $\sigma_U > \sigma_V > \sigma_W$. This appears to be the case for our dispersions (see Table 8). Also, σ_V/σ_U (0.70 for our sample) lies in the expected range from 0.55 to 0.70 (Wielen 1974) for old disk objects.

Figure 6 depicts the distribution of our sample's vector space velocity components relative to the LSR. The asymmetry in V is most likely a result of asymmetric drift (see Binney & Tremaine 1987). The asymmetry in U, however, is somewhat surprising because one would expect the average of U (and also W) to be symmetric about zero. In fact, Wielen (1974) suggested a method of determining the dispersions for each of the vector components, which involved normalizing each by the W-component. It is believed that any asymmetry in their original distributions should have

TABLE 8

UVW DA White Dwarf Space-Motion Comparison

Study Group[a]	Notes	U	σ_U	V	σ_V	W	σ_W	T	σ_T
SEA.....	1	23.1	40.6	−30.4	29.6	−11.8	25.4	62.7	28.8
A99	2	12.5	43.7	−25.4	34.3	−05.2	23.6	54.5	28.7
S90.....	3	−11.2	49	−28.7	35	−8.9	24	...	...
	4	−10.7	44	−26.4	31	−8.2	21	...	...
	5	−9.6	39	−25.6	27	−11.9	21	...	...

Notes.—(1) Fifty WDs, where $10.00 \lesssim M_v \lesssim 19.00$; (2) 256 WDs, where $10.00 \lesssim M_v \lesssim 16.00$; (3) inactive solar-type dwarfs; (4) all solar-type dwarf stars; (5) BY Draconis binaries.

[a] (SEA) Silvestri et al. 2000, this study; (A99) Anselowitz et al. 1999; (S90) Soderblom 1990.

been averaged out over their evolutionary timescales as the dispersion of the group increased.

Figure 7 depicts the WD velocities in the U-V plane, without (Fig. 7*a*) and with (Fig. 7*b*) the v_r component. The typical shape of the U-V plane with zero v_r assumption is asymmetric toward negative V values and fairly symmetric about U with respect to the LSR. This agrees well with those obtained by Sion & Oswalt (1988) and Sion et al. (1988) for a null radial velocity distribution of WDs. They are also similar to Upgren's (1978) U-V plane results for MS stars without Ca II emission, as well as U-V plane distributions of dwarf M stars given in Mihalas & Binney (1968). Curves of equal Galactocentric orbital eccentricity (Bottlinger curves from Eggen, Lynden-Bell, & Sandage 1962) are drawn for $e = 0.50$ and 0.75. All WD companions in our sample have $e \lesssim 0.5$, indicating that these stars are confined to orbits within the old disk of the Galaxy as opposed to the halo.

For the most part, the complete space-motion components we have generated for the DA members of CPMBs are in reasonable agreement (both in magnitude and sign) with the individual DA space motions computed with zero radial velocity by Sion et al. (1988). This similarity, within the errors, exists despite the inclusion of radial velocities and different values of photometric parallaxes used in this study. With but a few exceptions, the new complete motions do not change the assignment of population subcomponent membership existing before the inclusion of radial velocities in the vector components of the motion (see Fig. 8). The exceptions are the following: the DBA4 star WD 0615−591 appears to be a young disk ($v_t \sim 30$–60 km s^{-1}) member, the DA stars WD 1716+020 and WD 1743−132 both now appear to be members of the halo subcomponent ($v_t \sim 200$ km s^{-1}), the DBAZ star WD 1917−077 is now firmly a member of the old disk subcomponent ($v_t \sim 60$–150 km s^{-1}), the DBA3 star WD 2154−437 is now a potential halo member, and the DA8 star WD 2253−081 is now a candidate for the halo subcomponent.

Following the discussion of Anselowitz et al. (1999) on the relationship between total space velocity and cooling age, we have computed the cooling ages for 37 of the 41 WDs in our sample based on the model grid tabulations of Wood (1995), using our individual masses and $T_{\rm eff}$. We were unable to obtain four WD ages because of problems with the photometry and/or temperature estimates for these stars (see Table 4). Figure 9*a* shows no significant increase in total space motion with age. The slope and regression values for the best-fit line are nearly zero, contrary to the expected trend reported by Anselowitz et al. (1999). The

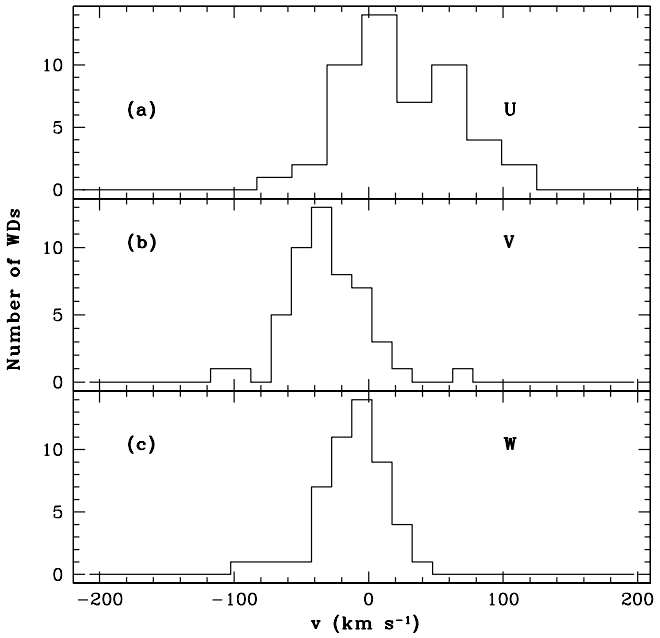

Fig. 6.—(*a*) U, (*b*) V, and (*c*) W velocity distribution in kilometers per second for the WDs. The mean values for each distribution are given in the text.

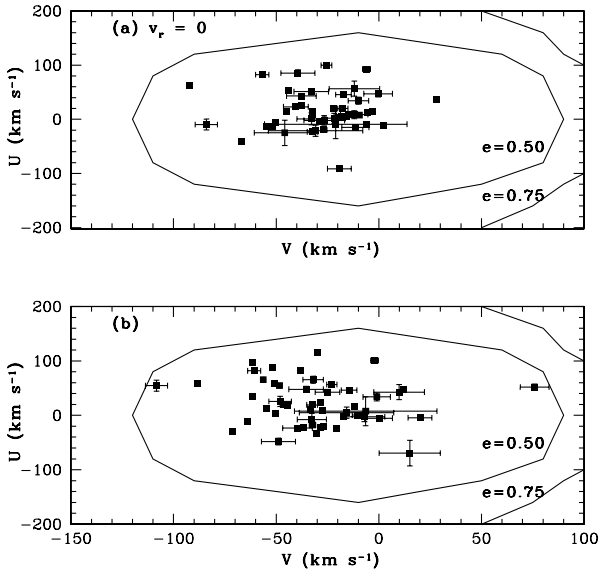

Fig. 7.—WDs in U- vs. V-velocity plane using (*a*) the null radial velocity ($v_r = 0$) assumption and (*b*) the radial velocities from Table 3. The curves in the figures represent the Galactocentric orbital eccentricities of 0.50 and 0.75 as labeled.

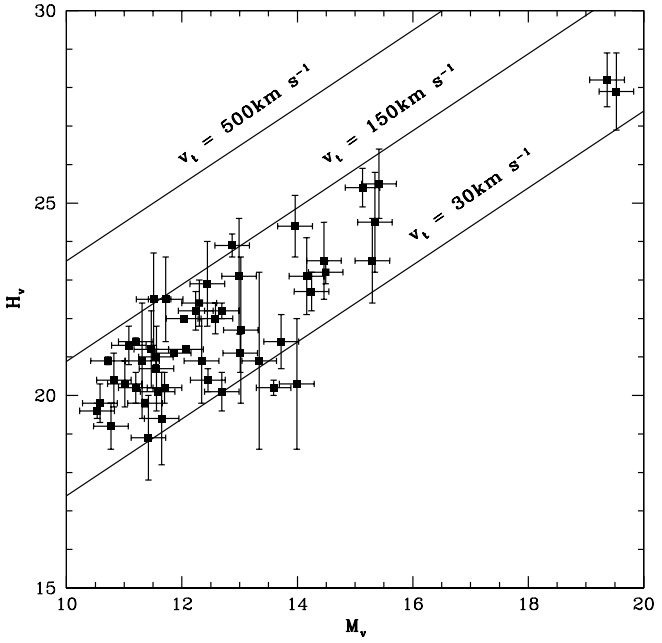

FIG. 8.—Reduced proper motion (H_v) vs. absolute magnitude (M_v) for all WDs with measured v_t. The plot suggests that most are old thick and thin disk stars. The mean tangential velocity is $\langle v_t \rangle = 72.9 \pm 4.8$ km s^{-1}.

mass versus cooling age plot (Fig. 9*b*) is also flat, especially if the five high-mass WDs are removed. As with Figure 9*a*, the slope and regression values are zero for the best-fit line.

Our inability to confirm the findings of Anselowitz et al. (1999) may be due to several factors. First, it is obvious from our mass distribution (Fig. 4) that there are two distinct groups of WDs in our sample based on Wilcoxon statistics discussed earlier. There is a clean separation of the five high-mass stars from the rest of the WDs in the sample shown in Figures 4, 5, and 9*b*. If these five high-mass WDs are the result of binary mergers, they will not necessarily follow the same cooling trend as a single WD. Also, our sample of cool WDs is deficient in hot WDs, so any temperature-dependent trend might not be evident amid the intrinsic scatter in mass. Also, as discussed in Wood (1992), unlike the mass, the cooling rates are sensitive to core composition and helium (He) mass layer thickness. The difference in ages between the predominantly carbon core sequences used in this study and those of pure oxygen composition results in a ~ 2 Gyr difference in WD ages, with the carbon sequences yielding older WDs (Wood 1992). Wood's models yield older ages for thinner He layers. At this point, we need to investigate the ages of these WDs using a variety of core compositions and He layer masses. We also need more young and old WDs to be able to comment definitively on the findings of Anselowitz et al. (1999).

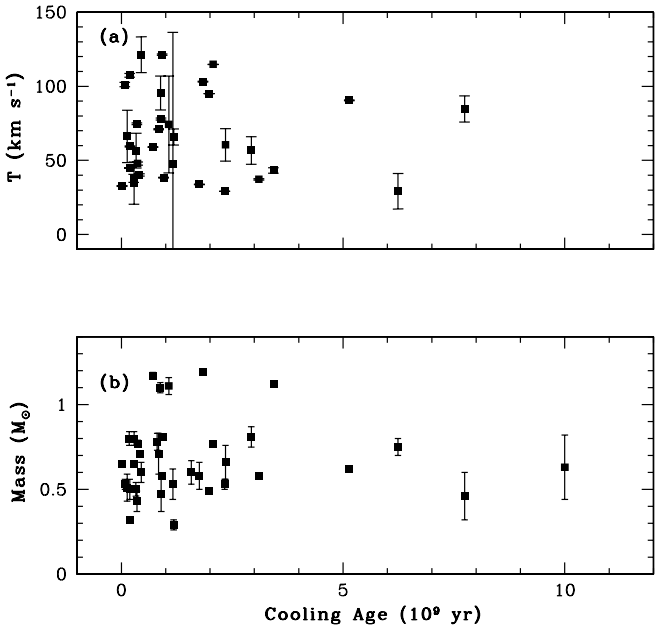

FIG. 9.—(*a*) Total space velocity (T) vs. cooling age and (*b*) the mass vs. cooling age for the WDs with measured gravitational redshifts.

7. CONCLUSIONS

The WD mass distribution reported here has several implications. First, it appears to have the highest mean mass determined by gravitational redshifts. However, the sample appears to be bimodal, suggesting a high-mass peak for cool WD stars around 1.2 $M_\odot$. The five high-mass stars in this sample skew the mean toward a higher mass, but the resulting mean when these stars are excluded is in good accord with prior studies of cool WDs. We cannot, at this point, distinguish between a true larger average mass for cooler WDs and averages that are overestimated because of the inclusion of high-mass WDs formed through binary mergers. Our study extends to cooler, fainter WDs than prior gravitational redshift studies; hence, it has been limited to modest S/N by the long integration times and size of the telescopes used. Clearly, much more time on telescopes larger than 4 m is necessary to further explore the cool regime of the WD mass distribution via gravitational redshifts.

There has been some speculation whether the method of gravitational redshifts yields larger masses on average than masses obtained by atmospheric studies. Koester (1987), Wegner & Reid (1991), Reid (1996), and this study all derived mass distributions using the gravitational redshift method. Combining the average mass distributions, v_g studies yield a mean mass $\langle M \rangle = 0.62 \pm 0.05\ M_\odot$. Koester et al. (1979), BSL, BLF, BRB, BRL, and FKB all used atmospheric line profile fitting to find the masses of WDs. The average mass of these six studies is $\langle M \rangle = 0.60 \pm 0.04\ M_\odot$. These two values are identical within the standard errors of the mean. Therefore, the mean mass obtained by atmospheric line profile fits is comparable to those obtained from gravitational redshift measurements even for relatively cool WDs *when velocities are tied to a standard system, sky subtraction is performed, and care is taken to eliminate systematic errors of measurement.* We have also shown that individual WD mass determinations are all too often inconsistent with other studies' measurements.

It is clear from our analysis of the space motions of CPMBs that our sample is typical of old, metal-poor, red dwarf stars in the thick disk population of the Galaxy. This is not surprising. Of particular interest is the identification of halo WDs. In our present sample there are only three WDs that appear to be potential halo candidates. A more robust analysis of their space motions will have to be undertaken to confirm this. Our average space-motion values are in accord with those of other groups, but much like individual mass determinations, individual WD space motions reported in the literature are typically inconsistent with our

study and with each other. It is not necessarily true that our sample of predominantly dM + WD binary pairs is representative of all CPMBs with a WD companion, as we have observed only pairs with measurable Hα. It is clear that there is a great need for more radial velocity measurements so that a robust analysis of the kinematics of WDs in binary systems can be performed. In particular, the kinematic study needs to include WDs that do not exhibit Hα to examine the possibility of kinematic differences between DA and non-DA WDs (Sion et al. 1988; Sion & Oswalt 1988). Sion & Oswalt (1988) have shown that DC WDs appear to have space motions that differ from other non-DA's and DA's. It would be interesting to explore this further with a larger sample of stars.

This study presents the first sizable body of complete space motions for WDs since the early studies of Greenstein & Trimble (1967). Our study also presents decidedly more precise radial velocities. However, any useful kinematic implications for late stellar evolution and WD progenitorship will not be realized until the complete space motions of non-DA WD spectroscopic subgroups can be compared with the DA sample. This comparative study must await the availability of radial velocities for a large body of non-DA spectroscopic types.

We thank Frank Valdez for many useful comments on data reduction techniques. Work was supported by National Science Foundation grant AST 90-16284 (T. D. O.), the NASA Astrophysics Theory Program through grant NAG 5-3103 (M. A. W.), and the NASA Graduate Student Researchers Program NGT 5-1086 (J. A. S.). We acknowledge use of the SIMBAD database, maintained by the CDS in Strasbourg, France. T. D. O. also wishes to thank the NSF for support through an internal grant from the Division of Astronomical Sciences.

REFERENCES

Adams, W. S. 1925, Proc. Natl. Acad. Sci., 11, 382
Anselowitz, T., Wasatonic, R., Mathews, K., Sion, E., & McCook, G. 1999, PASP, 111, 702
Barker, J. A. 1993, Master's thesis, Florida Inst. Technol.
Benvenuto, O. G., & Althaus, L. G. 1999, MNRAS, 303, 30
Bergeron, P., Liebert, J., & Fulbright, M. S. 1995, ApJ, 444, 810 (BLF)
Bergeron, P., Ruiz, M. T., & Leggett, S. 1997, ApJS, 108, 339 (BRL)
Bergeron, P., Saffer, R. A., & Liebert, J. 1992, ApJ, 394, 228 (BSL)
Bergeron, P., Wesemael, F., Fontaine, G., & Liebert, J. 1990, ApJ, 351, L21
Binney, J., & Tremaine, S. 1987, Galactic Dynamics (Princeton: Princeton Univ. Press)
Bragaglia, A., Renzini, A., & Bergeron, P. 1995, ApJ, 443, 735 (BRB)
Eggen, O. J., Lynden-Bell, D., & Sandage, A. R. 1962, ApJ, 136, 748
Finley, D. S., Koester, D., & Basri, G. 1997, ApJ, 488, 375 (FKB)
Fontaine, G., & Wesemael, F. 1987, in IAU Colloq. 95, Conference on Faint Blue Stars, ed. A. G. Davis Phillip, D. S. Hayes, & J. W. Liebert (Schenectady: L. Davis), 319
Giovannini, O., Kepler, S. O., Kanaan, A., Wood, M. A., Claver, C. F., & Koester, D. 1998, Baltic Astron., 7, 131
Grabowski, B., Madej, J., & Halenka, J. 1987, ApJ, 313, 750
Greenstein, J. L. 1982, ApJ, 252, 285
———. 1986, AJ, 92, 859
Greenstein, J. L., Boksenberg, A., Carswell, R., & Shortridge, K. 1977, ApJ, 212, 186
Greenstein, J. L., & Trimble, V. 1967, ApJ, 149, 283
Hamada, T., & Salpeter, E. E. 1961, ApJ, 134, 683
Hansen, B. 1999, ApJ, 520, 680
Iben, I., Jr., & Laughlin, G. 1989, ApJ, 341, 312
Iben, I., Jr., & Tutukov, A. V. 1984, ApJ, 284, 719
Koester, D. 1987, ApJ, 322, 852
Koester, D., & Reimers, D. 1989, A&A, 217, L1
Koester, D., Schulz, H., & Wegner, G. 1981, A&A, 102, 331
Koester, D., Schulz, H., & Weidemann, V. 1979, A&A, 76, 262
Leggett, S. K., Ruiz, M. T., & Bergeron, P. 1998, ApJ, 497, 294
Liebert, J., Dahn, C. C., & Monet, D. G. 1988, ApJ, 332, 891
Luyten, W. J. 1963, Proper Motion Survey with the 48-Inch Schmidt Telescope, Vol. 1 (Minneapolis: Univ. Minnesota)
———. 1969, Proper Motion Survey with the 48-Inch Schmidt Telescope, Vol. 21 (Minneapolis: Univ. Minnesota)
———. 1974, Proper Motion Survey with the 48-Inch Schmidt Telescope, Vol. 38 (Minneapolis: Univ. Minnesota)
———. 1979, Proper Motion Survey with the 48-Inch Schmidt Telescope, Vol. 51 (Minneapolis: Univ. Minnesota)
Marsh, T. R., Dhillon, V. S., & Duck, S. R. 1995, MNRAS, 275, 828
McCook, G. P., & Sion, E. M. 1999, ApJS, 121, 1
McMahan, R. K. 1989, ApJ, 336, 409
Mihalas, D., & Binney, J. 1968, Galactic Astronomy (2d ed.; New York: Freeman)
Oke, J. B., Weidemann, V., & Koester, D. 1984, ApJ, 281, 276
Oswalt, T. D., Hintzen, P. M., & Luyten, W. J. 1988, ApJS, 66, 391
Oswalt, T. D., Sion, E. M., Hintzen, P. M., & Liebert, J. W. 1990, in Proc. 7th European Workshop on White Dwarfs, ed. G. Vauclair & E. Sion (NATO ASI Ser. C, 336) (Dordrecht: Kluwer), 379
Oswalt, T. D., Smith, J. A., Wood, M. A., & Hintzen, P. 1996, Nature, 382, 692
Poveda, A., Herrera, M. A., Allen, C., Cordero, G., & Lavalley, C. 1994, Rev. Mexicana Astron. Astrofis., 28, 43
Provencal, J. L., Shipman, H. L., Hog, E., & Thejll, P. 1998, ApJ, 494, 759
Reid, I. N. 1996, AJ, 111, 2000
Saumon, D., & Jacobson, S. B. 1999, ApJ, 511, L107
Schmidt, G. D., Bergeron, P., Liebert, J., & Saffer, R. A. 1992, ApJ, 394, 603
Schulz, H. 1977, A&A, 54, 315
Shipman, H. L., & Mehan, R. G. 1976, ApJ, 209, 205
Silvestri, N. M. 1997, Master's thesis, Florida Inst. Technol.
Sion, E. M., Fritz, M. L., McMullin, J. P., & Lallo, M. D. 1988, AJ, 96, 251
Sion, E. M., & Liebert, J. 1977, ApJ, 213, 468
Sion, E. M., & Oswalt, T. D. 1988, ApJ, 326, 249
Smith, J. A. 1997, Ph.D. thesis, Florida Inst. Technol.
Soderblom, D. R. 1990, AJ, 100, 204
Upgren, A. R. 1972, AJ, 77, 745
———. 1978, AJ, 83, 626
Vennes, S., Fontaine, G., & Brassard, P. 1995, A&A, 296, 117
Vogt, S. S., et al. 1994, Proc. SPIE, 2198, 362
von Hippel, T. 1996, ApJ, 458, L37
Wegner, G. 1989, in IAU Colloq. 114, White Dwarfs, ed. G. A. Wegner (New York: Springer), 401
Wegner, G., & Reid, N. 1987, in IAU Colloq. 95, Conference on Faint Blue Stars, ed. A. G. Davis Phillip, D. S. Hayes, & J. W. Liebert (Schenectady: L. Davis), 649
———. 1991, ApJ, 375, 674
Wegner, G., Reid, N., & McMahan, R. K. 1989, in IAU Colloq. 114, White Dwarfs, ed. G. A. Wegner (New York: Springer), 378
Weidemann, V., & Koester, D. 1984, A&A, 132, 195
Weistrop, D. 1977, ApJ, 215, 845
Wielen, R. 1974, Highlights Astron., 3, 395
Wilson, R. E. 1963, General Catalogue of Stellar Radial Velocities (Washington: Carnegie Inst. Washington)
Winget, D., Hansen, C., Liebert, J., Van Horn, H., Fontaine, G., Nather, R., Kepler, S., & Lamb, D. 1987, ApJ, 315, L77
Wood, M. A. 1990, Ph.D. thesis, Univ. Texas Austin
———. 1992, ApJ, 386, 539
———. 1995, in Proc. 9th European Workship on White Dwarfs, ed. D. Koester & K. Werner (Lecture Notes Phys., 443) (New York: Springer), 41
Wood, M. A., & Oswalt, T. D. 1992, ApJ, 394, L53
Yuan, J. W. 1989, A&A, 224, 108